JSTR
ASEAN Journal of Scientific and Technological Reports

Research article

Plasma Instability During ITBs Formation with Pellet Injection in Tokamak

Ponkris Klaywittaphat[1*], Thawatchai Onjun[2], Roppon Picha[3], Jiraporn Promping[4] and Boonyarit Chatthong[5]

[1] Faculty of Engineering, Thaksin University, Phatthalung, Thailand; ponkris@hotmai.com
[2] Thailand Institute of Nuclear Technology, Bangkok, Thailand; Thawatchi.onjun007@gmail.com
[3] Thailand Institute of Nuclear Technology, Bangkok, Thailand; aeroppon@gmail.ac.th
[4] Thailand Institute of Nuclear Technology, Bangkok, Thailand; ame026@gmail.ac.th
[5] Division of Physical Science, Faculty of Science, Prince of Songkla University, Songkhla, Thailand; boonyarit.ch@psu.ac.th
* Correspondence: ponkris@hotmail.com

Abstract: JET H-mode plasma discharge 53212 simulation during the pellet fueling operation in the presence of an internal transport barrier is carried out using the 1.5D BALDUR integrated predictive modelling code. The plasma instability during ITB formation with pellet injection in a tokamak is investigated. These simulations use a neoclassical transport model and an anomalous transport model (either multimode or mixed Bohm/gyro-Bohm core transport model). The boundary condition is described at the top of the pedestal, which is calculated theoretically based on a combination of magnetic and flow shear stabilization pedestal width scaling and an infinite-n ballooning pressure gradient model. The toroidal flow calculation is based on the neoclassical viscosity toroidal velocity model. It was found that the shallower pellet does not destroy the ITB, which locating mainly between r/a = 0.8 and 0.9. Moreover, in the plasma center region (0.4<r/a<0.6) the effective electron thermal diffusivities do not change during the ablation time. However, the effective electron thermal diffusivities decrease after pellet ablation, which means a shallower pellet can improve the internal transport barrier.

Keywords: Plasma, Fusion, Pellet, Transport, Micro-instability, ITB

Citation:
Klaywittaphat, P.; Onjun, T.; Picha, R.; Promping, J.; Chatthong, B. Plasma Instability During ITBs Formation with Pellet Injection in Tokamak *ASEAN J. Sci. Tech. Report.* **2022**, *25*(4), 11-20. https://doi.org/10.55164/ajstr.v25i4.247569.

Article history:
Received: October 14, 2022
Revised: October 26, 2022
Accepted: October 27, 2022
Available online: November 20, 2022

1. Introduction

The progress in understanding plasma instability in a tokamak has been discussed for several decades in fusion research and development. Various theoretical modeling and numerical codes have been developed as a tool for this study [1–3]. Transport analysis of plasma discharges from different tokamaks under several conditions has resulted in a better understanding of their behaviors. It was found that the ion and electron thermal transports agree with theoretical predictions for turbulent transport due to gradient-driven drift-type micro-instabilities [4–6]. J. Weiland reported that the anomalous heat transport in the plasma core is mainly driven by a combination of Ion Temperature Gradient (ITG) and Trapped Electron Mode (TEM) instabilities [1]. A comprehensive assessment of transport behaviors also requires further experimental studies in various scenarios and the inclusion of complicated non-linear effects in those numerical studies.

Nevertheless, the results from the linear analysis still survive for an overall understanding [4]. Many useful and quantitatively correct conclusions can be obtained from a study based on a simplified drift-fluid description. These purely fluid models [2,5], or models with elements of gyro-motion [3] incorporated, show reasonable agreement with experiments and can describe many diverse observations.

A recent analytic study of the dissipative trapped electron instability in steep density and temperature gradients, such as those found experimentally in internal transport barriers (ITBs) in the Mega Ampere Spherical Tokamak (MAST) [7], showed that the growth rate of long-wavelengths of TEM for $k_\theta \rho_i < 0.5$ has a non-trivial dependence on collisionality. In particular, the limit of low collisionality, $\nu_{eff}/\omega << 1$, the TEM is stabilized by increasing collisionality. The result of Ref. [7] also showed the role of collisionality on drift instabilities. The effect of the pellet with micro instability in MAST can be seen in [8].

This work investigates the impacts of pellets on the ITBs and micro-stability analysis of the drift electrostatic waves, specifically ITG and TEM modes. A self-consistent simulation of JET H-mode discharge 53212 is carried out using the 1.5D BALDUR integrated predictive modeling code. In this simulation, the pellet ablation described using the neutral gas shielding (NGS) model with grad-B drift effect is taken into account. The NGS pellet model is coupled with a plasma core transport model, a combination of a neoclassical transport model NCLASS and an anomalous transport model (either The Multimode model (MMM) or Mixed Bohm/gyro-Bohm core transport model). The evolution of growth rate due to ITG and TEM modes is analyzed during the pellet fueling operation. This can result in a better understanding of plasma behaviors during pellet injection and ITBs formation.

This paper is organized as follows. Section 2 describes the details of models used in this work, including core transport and pellet models. The simulation results and micro instability analysis is carried out in Section 3. The conclusions are shown in Section 4.

2. Description of Models

2.1 MMM 95 anomalous transport model

The Multimode model (MMM) [6] is a combination of three theoretical based models, including the Weiland model for ion temperature gradient (ITG) and trapped electron modes (TEM), the Guzdar-Drake model for drift-resistive ballooning modes (RB), and a model for kinetic ballooning modes (KB). The effect of plasma elongation is also included by multiplying all the anomalous transport contributions to the Multimode model with κ^{-4}, producing the observed asymptotic scaling of confinement time and the best overall match to experimental data. The description of the Weiland model for toroidal geometry and circular, concentric magnetic surfaces is given in Ref. [5]. In brief, the ITG mode is provided by

$$\omega_{ri} = \frac{k_\theta \rho_s}{2L_{ni} m_i^{1/2}} T_e^{1/2} \left[1 - \frac{2L_{ni}}{R}\left(1 + \frac{10}{9}\frac{T_i}{T_e}\right)\right] \tag{1}$$

and

$$\gamma_i = \frac{2^{1/2} k_\theta \rho_s}{R m_i^{1/2}} T_i^{1/2} \sqrt{\frac{R}{L_{Ti}} - \frac{R}{L_{Ti,th}}}\,. \tag{2}$$

The TEM is given by

$$\omega_{re} = \frac{k_\theta \rho_s}{2L_{ne} m_e^{1/2}} T_e^{1/2} \left[K_t \left(1 - \frac{2L_{ne}}{R}\right) - \frac{20}{3}\frac{L_{ne}}{R}\right] \tag{3}$$

and

$$\gamma_e = \left(\frac{2K_t}{m_i}\right)^{1/2} \frac{k_\theta \rho_s}{R} T_e^{1/2} \sqrt{\frac{R}{L_{Te}} - \frac{R}{L_{Te,th}}}\,. \tag{4}$$

The diffusion coefficient for the $E \times B$ *1993* drift-resistive ballooning mode model by Guzdar and Drake [9] is

$$D^{RB} = 94q^2 \rho_e v_{ei} (-R\hat{\chi} \cdot \nabla p/p)\kappa^{-4}, \tag{5}$$

Where p is the plasma pressure and$\rho_e = v_{the}/\Omega_e$. A soft beta limit is approximated by the ''kinetic ballooning mode'' model, with the particle diffusion coefficient given by

$$D^{KB} = c_s p_s^2 (-R\hat{\chi} \cdot \nabla p/p) exp\left[3.5\,\beta'/\beta'_{c_1} - 1\right]\kappa^{-4}, \tag{6}$$

where $\beta' \equiv d\beta/dr$, and $\beta'_{c1} = r(dq/dr)/(1.7q^3R)$ is an approximation to the first ballooning mode stability limit. Then the thermal and particle transport coefficients can be expressed as [6]:

$$\chi_i = 0.8\chi_{i,ITG\&TEM} + 1.0\chi_{i,RB} + 1.0\chi_{i,KB} \tag{7}$$

$$\chi_e = 0.8\chi_{e,ITG\&TEM} + 1.0\chi_{e,RB} + 1.0\chi_{e,KB} \tag{8}$$

$$D_H = 0.8D_{H,ITG\&TEM} + 1.0D_{H,RB} + 1.0D_{H,KB} \tag{9}$$

$$D_Z = 0.8D_{Z,ITG\&TEM} + 1.0D_{Z,RB} + 1.0D_{Z,KB} \tag{10}$$

where χ_i is the ion thermal diffusion coefficient in the unit of m²/s, χ_e is the electron thermal diffusion coefficient in the unit of m²/s, D_H is hydrogenic particle diffusion coefficient in the unit of m²/s and D_Z is impurity particle diffusion coefficient in the unit of m²/s.

2.2 Mixed Bohm/gyro-Bohm anomalous transport model

The Mixed Bohm/gyro-Bohm (Mixed B/gB) anomalous transport model [10-11] is semi-empirical. Both the electron and ion thermal diffusivities consist of two terms. The diffusivity of the Bohm term can be written as:

$$\chi_B = \alpha_B R \left|\frac{\nabla(n_e T_e)}{n_e B_\emptyset}\right| q^2 \tag{11}$$

With the constant α to be determined empirically. However, evidence from JET suggests that the Bohm term should also depend on the temperature gradient near the plasma edge. Consequently, Bohm scaling has a final form as follows:

$$\chi_B = 4 \times 10^{-5} R \left|\frac{\nabla(n_e T_e)}{n_e B_\emptyset}\right| q^2 \left(\frac{T_e(0.8\rho_{max}) - T_e(\rho_{max})}{T_e(\rho_{max})}\right), \tag{12}$$

The Gyro-Bohm term can be written as

$$\chi_{gB} = 5 \times 10^{-6} \sqrt{T_e} \left|\frac{\nabla(T_e)}{B_T^2}\right|. \tag{13}$$

The anomalous ion and electron thermal diffusivities are constructed from the sum of these Bohm and gyro-Bohm terms, with empirically determined coefficients:

$$\chi_i = 0.5\chi_{gB} + 4.0\chi_B, \tag{14}$$

$$\chi_e = 1.0\chi_{gB} + 2.0\chi_B. \quad (15)$$

The hydrogenic and impurity-charged particle diffusivity is given by

$$D_H = D_Z = (0.3 + 0.7\rho)\frac{\chi_e\chi_i}{\chi_e+\chi_i}. \quad (16)$$

2.3 NCLASS neoclassical transport model

Neoclassical ion thermal transport is computed using the NCLASS module [12]. The NCLASS module calculates the neoclassical transport properties of multi-species axisymmetric plasma of arbitrary aspect ratio, geometry, and collisionality, by solving the radial and parallel force balance equations for the flows within a flux surface using multiple species, reduced charge state approach given in Ref. [13]. The radial fluxes in the banana regime are related to these flows and the neoclassical viscosities. The bootstrap current and electrical resistivity are also derived from these flows. The classical and Pfirsch-Schlüter fluxes and those driven by a user-specified parallel force are also calculated. The viscosities are calculated by numerically integrating over velocity space and are continuous over all collisionality regimes and aspect ratios. In addition, other effects, including banana orbit squeezing, potato orbit effects, and additional force terms to accommodate neutral beam, charge exchange, toroidal field ripple, and anomalous toroidal drag forces, are included.

2.4 NGS ablation model and relocation model

Two simultaneous processes can occur during each pellet, including pellet ablation and mass relocation. The neutral gas shielding (NGS) model [2] is used, in which an ablation rate of this model can be expressed in terms of the power function as follows:

$$\frac{dN}{dt} = 5.2 \times 10^{16} n_e^{0.333} T_e^{1.64} r_p^{1.333} M_i^{-0.333} \quad (17)$$

Where N, n_e (m^{-3}), T_e (eV), r_p (m), and M_i (u) are the number of particles in a pellet, electron density, electron temperature, pellet radius, and pellet mass, respectively. For the mass relocation model, a scaling model of pellet drift displacement, based on the grad-B induced pellet drift [14, 15], has been considered. The developing of the scaling law for grad-B Drift [14], based on a set of ~800 simulations with varying injection and plasma target parameters in the vicinity of typical tokamak configurations (~ ±40% of standard parameter settings), least square fits have been carried out to determine the main parameter dependencies and to derive an equation for the rough calculation of the absolute average particle drift displacement in terms of the flux coordinate $(R_{max} - R_{min})/2$:

$$\Delta_{\text{Drift}} = C_1 \left(\frac{V_p}{100}\right)^{C2} r_p^{C_3} n_{e0}^{C_4} T_{e0}^{C_5} (\|\alpha| - C_6| + C_8)^{C_7} \times (1-\Lambda)^{C_9} a_0^{C_{10}} R_0^{C_{11}} B_0^{C_{12}} \kappa^{C_{13}} \quad (18)$$

With injection velocity V_p (m/s), pellet radius r_p (mm), axial density n_{e0} (10^{19} m^{-3}) and electron temperature T_{e0} (keV), injection angle $\alpha \in [-\pi, \pi]$, impact parameter of the pellet trajectory Λ (norm. minor radius), minor radius a_0 (m), major radius R_0 (m), toroidal field B_0 (T), and plasma elongation κ. To avoid statistical artifacts in the calculation coming from the rational q-surface effect on the drift-damping behavior, which cannot easily be described as part of a scaling fit formula, the q-profile was changed arbitrarily for each simulation run ($q_{edge} \in [3,9]$). Only pellets ablated before reaching the tangency point of the trajectory with the flux surfaces were considered. The results and root mean square (rms) errors obtained for the constants C_1-C_{13} for two different assumptions concerning the parameter space to be analyzed summarized in [14].

3. Simulation Results and Micro Instability Analysis

The summary of the basic plasma parameters and summary of the pellet injection parameters used in JET discharge 53212 a target, a plasma was chosen at I_p/B_t = 2.5 MA/2.4 T with $\delta \approx 0.34$ showing a confinement collapse when trying to raise the density beyond $n/n_{GW} = 0.8$ with strong gas puffing. In such a plasma solid 4 mm^3 deuterium cubes were launched at a speed of 160 m s^{-1} from the high field side downward at an angle of 44° with respect to the horizontal plane and with a tangency radius at a normalized minor radius $\rho \sim 0.6$–0.7. The optimization strategy translated into launching a first pellet string at 6 Hz to raise the density, followed by a pellet string at 2 Hz, which is sufficiently slow to allow confinement recovery after each pellet, shown in table 2 and table 3 of [25].

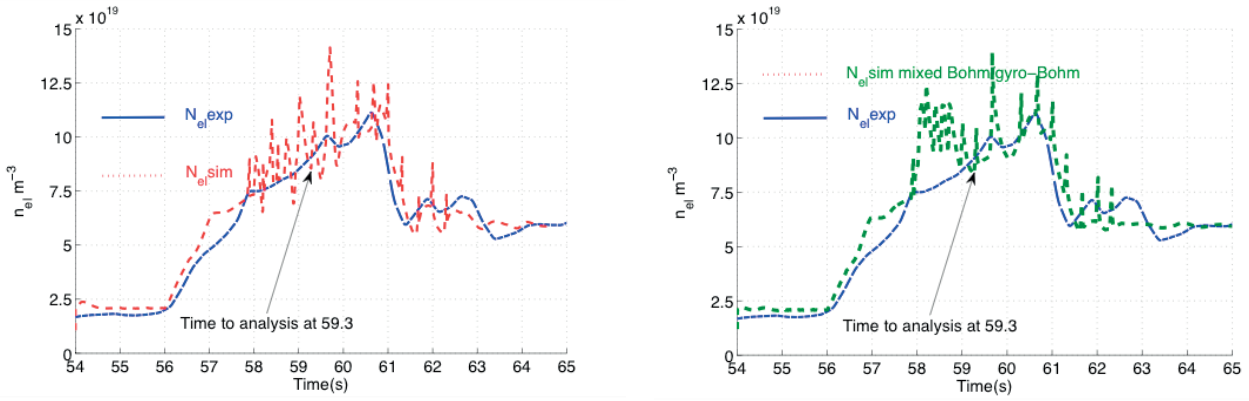

Figure 1. The time evolution of line average electron density is compared for experimental data and the simulations using either MMM95 (left) or Mixed Bohm/gyro-Bohm (right) [25].

Figure 1 compares an evolution of line average electron density obtained from the experiment and the simulations using the MMM95 transport model (left panel) and Mixed B/gB model (right panel). It can be seen in both panels that the line average electron density rises quickly after the pellet's launching. Both simulations tend to agree with experimental data, especially the simulation using the MMM95 transport model, which yields better agreement during the early period of pellet operation due to the off-diagonal elements of the transport matrix in the Weiland model, providing the convective flux adequate to reproduce the observed density profile peaking [22], which can be seen in Figure 1. At the later time of pellet operation, both simulations yield similar agreement with experimental data.

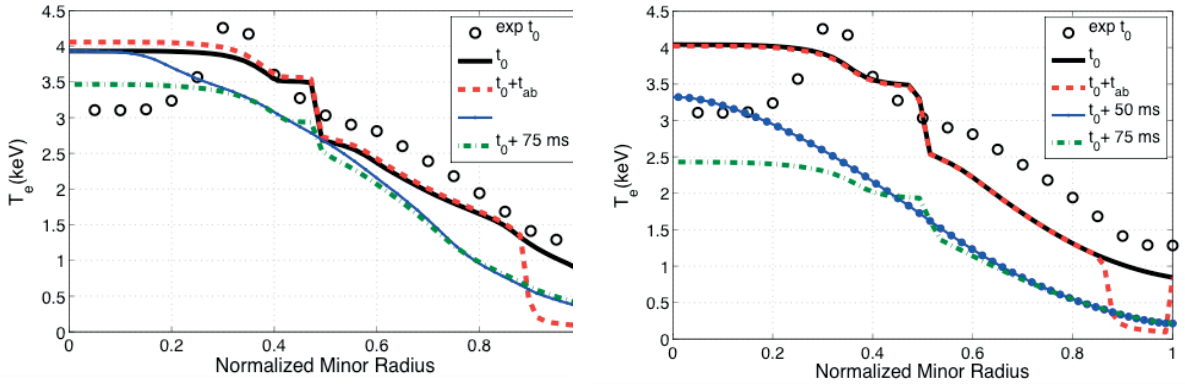

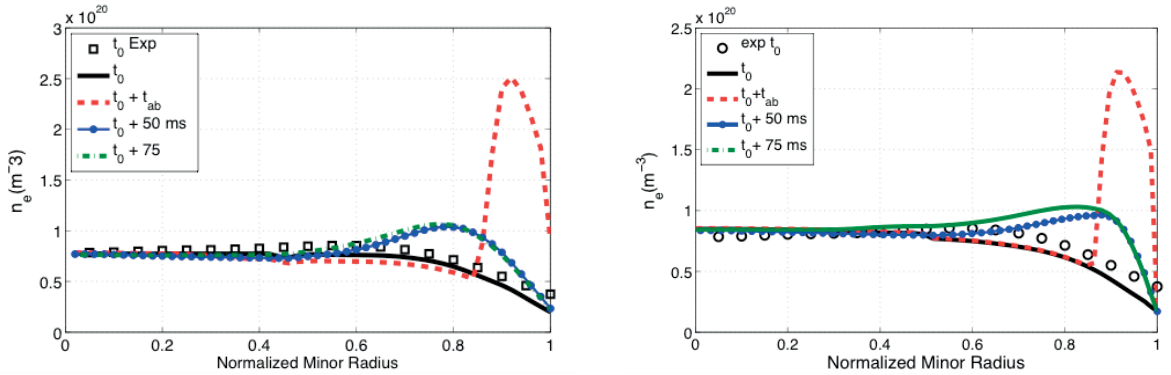

Figure 2. The electron temperature and density profiles during the pellet operation are plotted for the experimental data and the simulations using MMM95 (left) and Mixed Bohm/gyro-Bohm (right) [25].

Figure 2 shows the profile comparison between the experimental data and simulation using the MMM95 transport model (left panels) and Mixed B/gB model (right panels) for electron density and electron temperature at 59.3 sec. Note that this is during pellet operation. The first pellet is launched at a time of 57.87 sec. The simulations are shown at different times during the pellet perturbation, including time t_0 referring to the time before pellet injection, $t_0 + t_{ab}$ referring to the time during pellet ablation, t_0 + 50 ms referring to the time at 50 ms after pellet launching (during relaxation process), and t_0 + 75 ms referring to a time at 75 ms after pellet launching (at the end of the relaxation process). It can be seen at the time before pellet injection that both predicted electron density and temperature agree with experiment data. For the electron density, a new peak of electron density is formed after pellet injection. Consequently, plasma starts to relax by transporting density inwards and outward. It can also be seen the electron density relaxes faster at the plasma edge than at the plasma core because the electron transport density at the plasma edge region is increased. It is worth noting that there is an off-axis peak of the electron temperature profile at r/a = 0.35 in the experimental profile and a large gradient of the electron temperature profile at r/a =0.5 in both simulation results. It should be mentioned on the origin of these irregularities. These resulted from the off-axis and NBI heating used in the experiment and simulations.

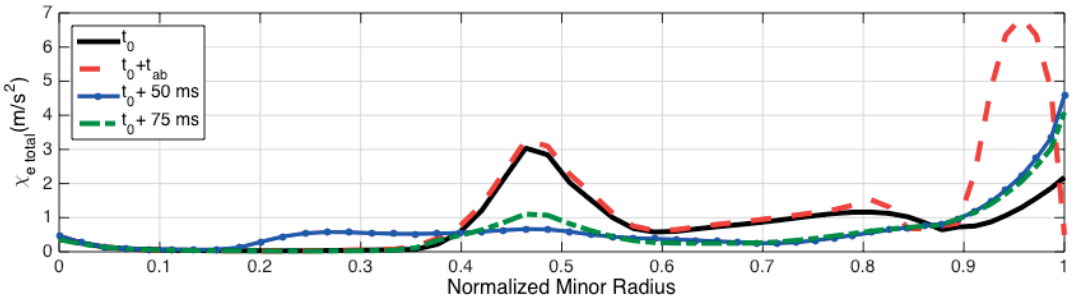

Figure 3. The profiles for total electron thermal diffusivity during the pellet operation are plotted for the simulations using MMM95.

Figure 3 shows the effective electron thermal diffusivities at different times during pellet operation. The panels show the results obtained from the simulation using the MMM95 transport model. It can be seen that the effective electron thermal diffusivities increase, especially in the region of pellet ablation ($0.8<r/a<1$). However, they decrease to levels similar to those before pellet injection in the plasma center region ($0.4<r/a<0.6$), and the effective electron thermal diffusivities do not change during the ablation time. However, the effective electron thermal diffusivities decrease after pellet ablation, which means a shallower pellet does not destroy the internal transport barrier because the electron thermal diffusivities in this area are not affected by a shallower pellet.

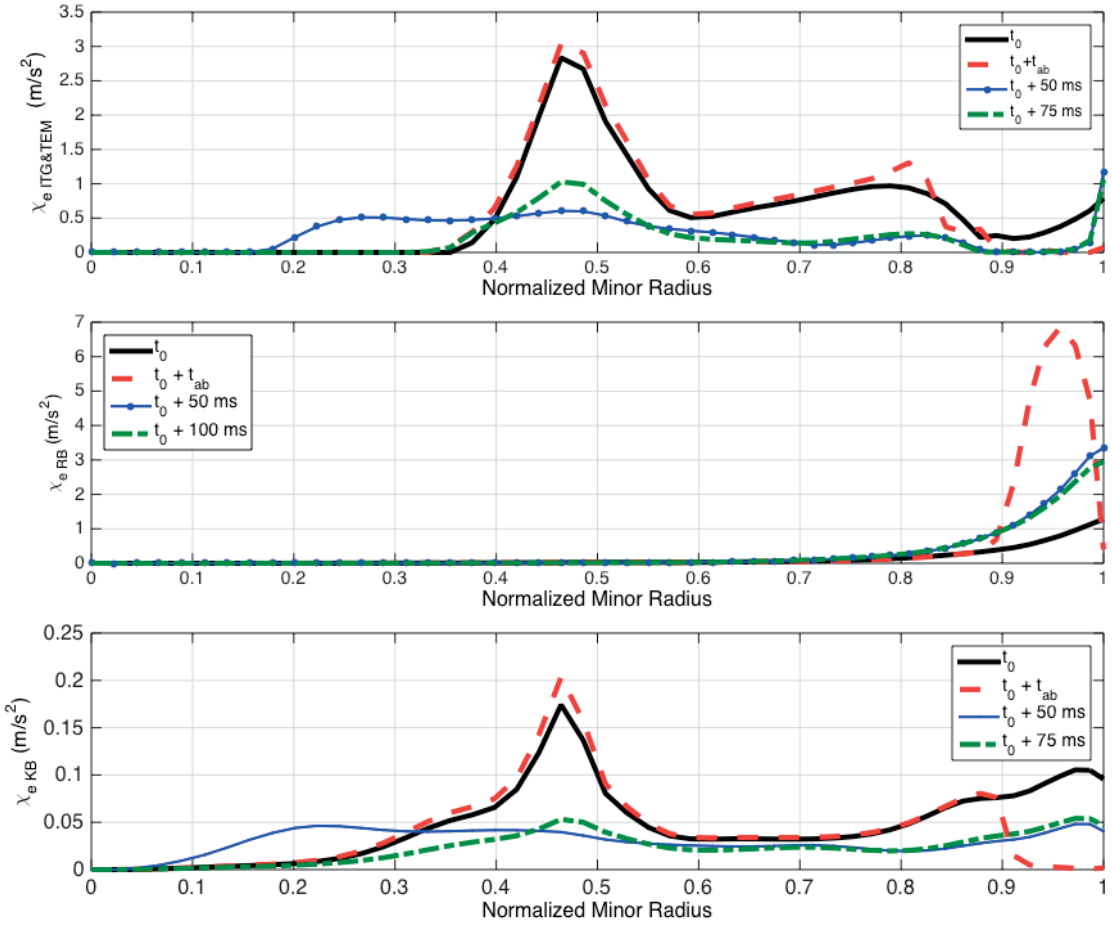

Figure 4. The components of electron thermal diffusivity profiles during the pellet injection obtained from the simulation using the MMM95 transport model are shown for the radius from ϱ = 0 to ϱ = 1.0. Those components are the drift wave (ITG&TE) (top panel), the drift-resistive ballooning (RB) modes (middle panel), and the kinetic ballooning (KB) modes (bottom panel).

Figure 4 shows the components of electron thermal diffusivities during the pellet injection obtained from the simulation using the MMM95 transport model. Those components are the drift wave (ITG&TEM), drift-resistive ballooning (RB) modes, and kinetic ballooning (KB) modes. It can be seen that the ITG&TEM component is dominant throughout the plasma, except near the plasma edge, in which the electron thermal diffusivities are dominated by both ITG&TEM and RB components. It can be noticed that right after a pellet enters the plasma, the ITG&TEM component remains almost the same, except for a reduction in the region near the plasma edge where another density peak is formed. Therefore, a reduction in the ITG&TEM component occurs throughout the plasma. This behavior also occurs for the KB component. For the RB component, right after a pellet enters the plasma, the RB component remains almost the same in the plasma core, except for a large increase near the plasma edge where another density peak is formed. This is caused by increased collisionality and resistivity near the plasma edge. Thus, it relaxes to the level before pellet injection.

Figure 5 shows the time evolution of electron density and temperature during pellet ablation. It can be seen that the electron density suddenly increases after pellet injection, but the electron temperatures rapidly drop. It is known that based on fluid concepts, an increase in the density gradient can stabilize the ion temperature gradient modes by decreasing the parameter $\eta_i = (\nabla T_i / T_i)/(\nabla n_i / n_i)$. However, in a gyrokinetic calculation for a density peaking case, it is found to be destabilizing [23]. Therefore, the stabilizing role of

density peaking depends on the actual fraction of trapped electrons and plasma collisionality. An increase of α ($\alpha = -q^2\beta R\nabla P/P$) can stabilize part of the microturbulence [24].

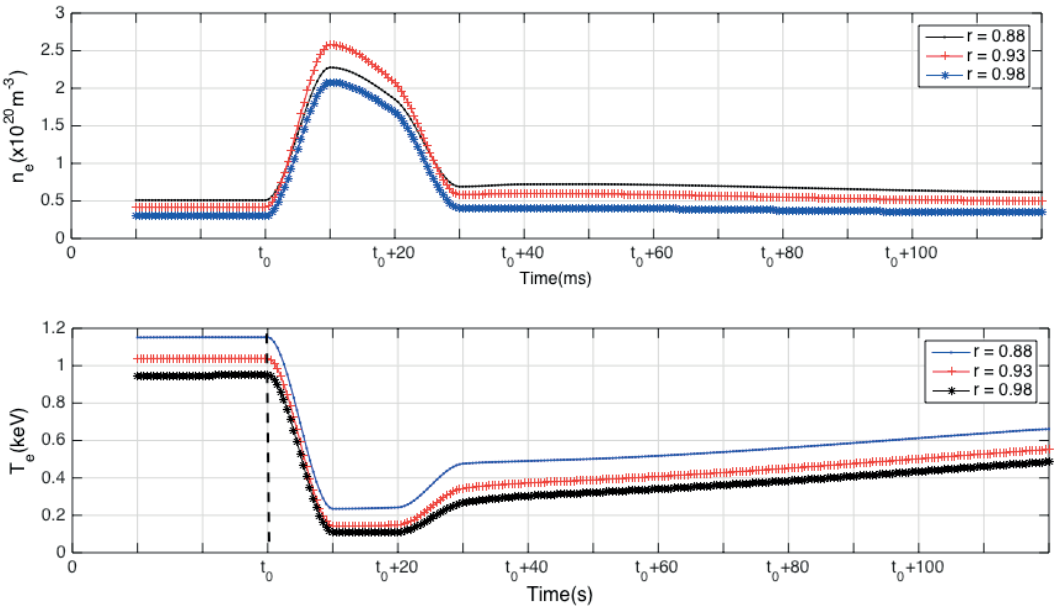

Figure 5. The time evolution of electron density, electron temperature, during pellet ablation.

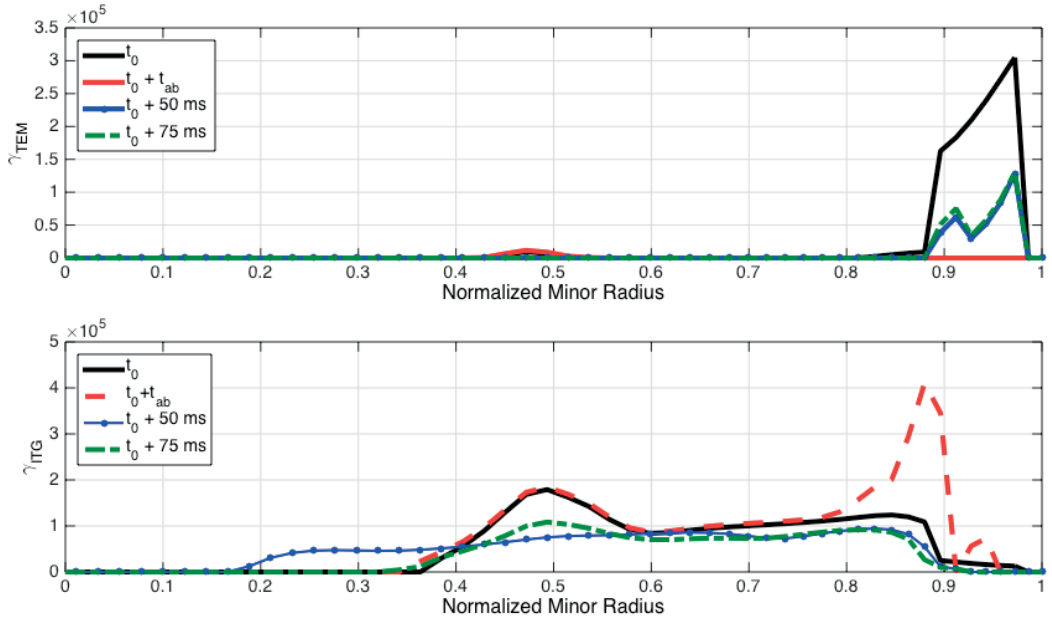

Figure 6. The profiles of the growth rate (s^{-1}) due to ITG and TEM during the pellet fueling operation are shown for the radius from ϱ = 0 to ϱ = 1.0.

Figure 6 shows the maximum growth rate for ITG and TEM modes during the pellet injection obtained from the simulation using the MMM95 transport code. At (r=0.88), the ITG growth rate increases immediately after pellet injection t_0+t_{abl}. The ITG modes can be stabilized by the increased density gradient and the decreased ion temperature gradient. However, the strong increase of ion temperature gradient at this time tends to destabilize the ITG growth rate. For the trapped electron modes (TEM) immediately after pellet

injection (t_0+t_{abl}). The TEM growth rate is decreased due to an increase in electron collisionality. Then, the growth rate recovers to the primary state at the middle location of the peak due to the pellet ablation profile, where (r=0.93). Immediately after pellet injection t_0+t_{abl}, we observe an initial decrease in the growth rate of TEM and a simultaneous increase in the growth rates of ITG. At this time, electron collisionality increases significantly, suppressing TEM growth rates. During the relaxation of the pellet deposition profile (t = t_0+50 ms), the growth rate based on TEM increases from the last time while the growth rate based on ITG mode drops at this time, and at t = t_0+50 ms, all profiles recover to the first state. At the outer surface (r=0.98), after the pellet ablation (at t = t_0 +50 ms), the growth rates and the complete stabilization of modes ITG and TEM are reduced. This suggests that in lower collisionality plasmas, the post-pellet may be unstable to TEM and ITG. It can also be seen that ITG modes dominate before pellet injection and are increased by the increased temperature gradient. TEM modes are stabilized by increased collisionality during pellet injection.

4. Conclusions

JET H-mode plasma discharge 53212 is carried out during the pellet fueling operation in the presence of an internal transport barrier (ITB) using the 1.5D BALDUR integrated predictive modelling code. It was found that the perturbation due to each pellet results in a change in thermal transport, especially in the resistive ballooning modes due to the increase of collisionality and resistivity near the plasma edge. It was found that the shallower pellet does not destroy the internal transport barrier, which locating mostly between r/a = 0.8 and 0.9. Moreover, in the plasma center region (0.4<r/a<0.6), the effective electron thermal diffusivities during the ablation time do not change. However, the effective electron thermal diffusivities decrease after pellet ablation, which means a shallower pellet can improve the internal transport barrier. A strong perturbation in the plasma causing a sudden change of thermal transport can be observed after each pellet enters the plasma. The results show that the micro-instability properties of the post-pellet profiles are highly sensitive to rapid and large excursions in the gradients, β_e and collisionality induced by the pellet injection. In particular, at a location corresponding to the part of the pellet deposition profile, ITG modes are destabilized by an increase in a temperature gradient, and TEM modes are stabilized by increased collisionality. The dominant mode in the simulation's pellet ablation region with the MMM95 core transport model is the resistive ballooning mode due to increased collisionality and resistivity near the plasma edge.

5. Acknowledgements

This work was partly supported by the International Atomic Energy Agency (IAEA) under contract No. 22785 and TSRI Fundamental Fund project number 91525. This work is a collaborative research project under the Center for Plasma and Nuclear Fusion Technology (CPaF).

References

[1] Manfredi, G.; Dendy, R.O. *Transport properties of energetic particles in a turbulent electrostatic field. Phys. Plasmas*, 1997, 4, 628.

[2] Parks, P. B.; Turnbull, R.J. *Effect of transonic flow in the ablation cloud on the lifetime of a solid hydrogen pellet in a plasma. Phys. Fluids*, 1978, 21, 1735.

[3] Singer, C.E. et al. .*Baldur: A one-dimensional plasma transport code.* Comput. Phys. Commun. 1988, 49 275

[4] Connor, J. W. et al. *Stability of the trapped electron mode in steep density and temperature gradients Plasma Phys. Controlled Fusion* ,2006, 48, 885.

[5] Weiland, J. *Collective modes in inhomogeneous plasma: kinetic and advanced fluid theory. Bristol: Institute of Physics Publishing,* 2000.

[6] Bateman, G. et al. *Predicting temperature and density profiles in tokamaks*. *Physics of Plasmas,* 1998, 5, 1793.

[7] Akers, R. J. et al *Transport and confinement in the Mega Ampère Spherical Tokamak (MAST) plasma. Plasma Phys. Control. Fusion,* 2003, 45, A175.

[8] Garzotti, L. et al. *Microstability analysis of pellet fuelled discharges in MAST Plasma Phys. Control. Fusion.*2014, 56, 035004.

[9] Guzdar, P. N. et al. *Shear flow generation by drift waves revisited. Physics of Fluids B*,1993, 5, 3712.
[10] M Erba et al. *Development of a non-local model for tokamak heat transport in L-mode, H-mode and transient regimes*, *Plasma Phys. Control. Fusion,* 1997, 39 261.
[11] Onjun, T. et al. *Comparison of low confinement mode transport simulations using the mixed Bohm/gyro-Bohm and the Multi-Mode-95 transport model. Physics of Plasmas*, 2001, 8, 975.
[12] Houlberg, W. A. et al. *Bootstrap current and neoclassical transport in tokamaks of arbitrary collisionality and aspect ratio*. *Phys. Plasma* , 1997 ,4, 3230.
[13] Hirshman, S. P. et al. *Neoclassical transport of impurities in tokamak plasmas. Nucl. Fusion,* 1981, 21, 1079
[14] Köchl, F. et al. *Pellet Drift Modelling – Validation and ITER Predictions, in Proc. 35th EPS Conf. Plasma Phys.* 32D P-4.099, 9–13 June 2008, Hersonissos, Greece.
[15] Pégourié, B. et al. *Homogenization of the pellet ablated material in tokamaks taking into account the ∇B-induced drif*. Nucl. Fusion, 2007, 47, 44.
[16] Parks, P. B. et al. *Effect of Parallel Flows and Toroidicity on Cross-Field Transport of Pellet Ablation Matter in Tokamak. Plasmas*,*Physical Rev Letters*, 2005, 94, 125002.
[17] Hannum, D. et al. *Comparison of high-mode predictive simulations using Mixed Bohm/gyro-Bohm and Multi-Mode (MMM95) transport models*. *Physics of Plasmas*,2001, 8, 965.
[18] Bateman, G. et al. *Integrated predictive modeling of high-mode tokamak plasmas using a combination of core and pedestal models. Physics of Plasmas,* 2003 ,10, 4358.
[19] Snyder, S. et al. *Effect of isotope mass on simulations of the high-mode pedestal and edge localized modes. Physics of Plasmas* 2005,12 112508
[20] Poolyarat, N. et al. *Simulation study of HL-2A-like plasma using integrated predictive modeling code. Plasma Physics Reports* ,2009,35,987.
[21] Chatthong, B. et al. *Model for toroidal velocity in H-mode plasmas in the presence of internal transport barriers. Nuclear Fusion*, 2010, 50(6), 064009.
[22] Garzotti, L. et al. *Particle transport and density profile analysis of different JET plasmas Nucl. Fusion.* 2003, 43, 1829.
[23] Romanelli, M. et al. *Effects of high density peaking and high collisionality on the stabilization of the electrostatic turbulence in the Frascati Tokamak Upgrade*. *Phys. Plasmas,* 2004 ,11 3845.
[24] Bourdelle, C. et al. *Impact of the α parameter on the micro stability of internal transport barriers*. *Nucl. Fusion,* 2005 ,45, 110.
[25] Klaywittaphat, P.; Onjun, T. *Transport and micro-instability analysis of JET H-mode plasma during pellet fueling*. *Nucl. Fusion,* 2017,57 022008.